High-Resistance Connection Detection in Permanent Magnet Synchronous Machine Using Zero-Sequence Current Component

Jun Hang, *Student Member, IEEE*, Jianzhong Zhang, *Member, IEEE*, Ming Cheng, *Fellow, IEEE*, Bangfu Zhang, *Student Member, IEEE*, and Shichuan Ding, *Member, IEEE*

***Abstract*—This paper focuses on the development of an online method for diagnosing high-resistance connection (HRC) in delta-connected permanent magnet synchronous machine (PMSM) using zero-sequence current component (ZSCC). The development of this method begins with the establishment of the mathematic model of the PMSM with the HRC. Based on the model, a ZSCC-based method is proposed to diagnose the HRC. The fault indicator and angle differences are defined for fault diagnosis. To implement online diagnosis, an effective frequency tracking algorithm is applied. Finally, the fault diagnosis steps are presented. This method is capable of detecting the fault, evaluating the fault severity, and identifying the faulty phases. The simulation and experiment are carried out to verify the proposed method. Both the results show the validity of the proposed method, leading to the effective diagnosis of the HRC in the delta-connected PMSM.**

***Index Terms*—Fault diagnosis, frequency tracking algorithm, high-resistance connection (HRC), permanent magnet machine, wind energy.**

I. Introduction

In recent decades, permanent magnet synchronous machine (PMSM) has been taken great concerns in wind energy conversion system (WECS) [1] and transportation, such as subway [2], owing to its high efficiency and high power density. In these occasions, an undetected fault or failure of the PMSM could lead to very high repair or replacement cost, or even catastrophic system failure. Therefore, fault detection is of great importance, which may help in scheduling preventive maintenance to avoid machine failure [3], [4].

The high-resistance connection (HRC) is one of the most common failures in the ac machines, where the phase resistance is increased, while the phase inductance is unvaried [5], [6]. This fault may be caused by a combination of poor workmanship, thermal cycling, and vibration, or damage of the contact surfaces due to pitting, corrosion, or contamination. This fault may produce one or more of the following symptoms: unbalance stator voltages and currents, increased torque pulsation, decreased average torque, increased losses, and excessive heating [6]. Consequently, if the fault is not detected in time, it may lead to the insulation damages to the machine [7]. Recently, many methods have been proposed to diagnose the HRC in the induction machine [5]–[10]. The dominant method among them is the machine current signature analysis, which is based on the analysis of the spectral contents of the stator currents [10]. Likewise, the HRC can be generated in the wide-used PMSM. However, to the best of the authors' knowledge, the previous literatures mostly focus on detection of the interturn fault [11]–[13], eccentricity fault [14], [15], and demagnetization fault [16], [17] in the PMSM rather than the HRC, in addition to [18]. In [18], two methods are proposed to detect the HRC. One method is based on the stator current, where the third-harmonic component of the stator current is used to detect the HRC. The other one is based on zero-sequence voltage components (ZSVC), where the HRC is detected by monitoring the fundamental component of the ZSVC. However, both the methods are not suitable for the diagnosis of the HRC in the PMSM with delta-connected windings since the third-harmonic component is already present in the stator current, and a neutral point is difficult to access. As known, the wye-connected and delta-connected windings are both common in the ac machine [19]–[21]. Hence, fault detection toward the delta-connected PMSM is also necessary. However, the delta-connected PMSM with the HRC is rarely studied so far. Hence, this paper aims to fill this gap, focusing on online diagnosis of HRC in the delta-connected PMSM.

This paper first proposes an online method for diagnosing the HRC in the delta-connected PMSM using zero-sequence current component (ZSCC). In the proposed method, a theoretical analysis is presented to obtain the expression of the ZSCC. The fault indicator and angle differences are defined, and an effective frequency tracking algorithm is applied. In this method, not only the HRC can be detected, independently of the phases in which the fault occurs, but also the faulty phases and fault severity can be determined.

Manuscript received January 17, 2015; revised May 14, 2015; accepted September 11, 2015. Date of publication September 17, 2015; date of current version January 28, 2016. This work was supported in part by the National Key Basic Research Program of China (973 Program) (2013CB035603) and the National Natural Science Foundation of China (51137001, 51320105002). Recommended for publication by Associate Editor J. Hur.

The authors are with the School of Electrical Engineering, Southeast University, Nanjing 210096, China (e-mail: jun_hang511@163.com; jiz@seu.edu.cn; mcheng@seu.edu.cn; bangfukuang@126.com; dingsc@126.com).

Color versions of one or more of the figures in this paper are available online at http://ieeexplore.ieee.org.

Digital Object Identifier 10.1109/TPEL.2015.2479846

II. Delta-Connected PMSM Model With HRC

In a three-phase healthy PMSM, the stator resistances of the three phases are nearly identical. As the HRC occurs, the stator resistance is imbalanced, and the HRC may be modeled by adding an additional resistance connected in series with one phase winding [7], as shown in Fig. 1. Suppose the saturation is neglected and other faults are not generated, the voltage

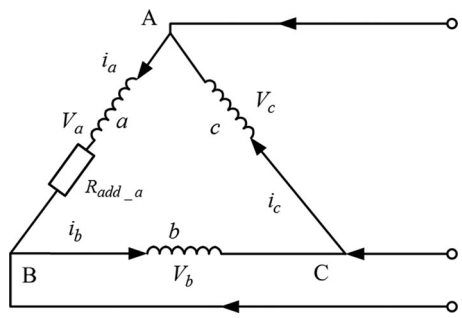

Fig. 1. Equivalent model of a delta-connected PMSM with HRC in phase *a*.

equations for a three-phase delta-connected PMSM with the HRC in the phase *a* are expressed as

$$\begin{bmatrix} V_a \\ V_b \\ V_c \end{bmatrix} = \begin{bmatrix} R_s + R_{\mathrm{add\_}a} & 0 & 0 \\ 0 & R_s & 0 \\ 0 & 0 & R_s \end{bmatrix} \begin{bmatrix} i_a \\ i_b \\ i_c \end{bmatrix} + \begin{bmatrix} L & M & M \\ M & L & M \\ M & M & L \end{bmatrix} \frac{d}{dt} \begin{bmatrix} i_a \\ i_b \\ i_c \end{bmatrix} + \frac{d}{dt} \begin{bmatrix} \lambda_{\mathrm{PM},a} \\ \lambda_{\mathrm{PM},b} \\ \lambda_{\mathrm{PM},c} \end{bmatrix} \quad (1)$$

where V_a, V_b, and V_c are the phase voltages, i_a, i_b, and i_c are the phase currents, R_s is the stator phase resistance, *L* is the stator phase self-inductance, *M* is the mutual-inductance between the stator phases, $R_{\mathrm{add\_}a}$ is the additional resistance in the phase *a*. $\lambda_{\mathrm{PM},a}$, $\lambda_{\mathrm{PM},b}$, and $\lambda_{\mathrm{PM},c}$ are the flux in the phases *a*, *b,* and *c* due to permanent magnets, respectively. They are expressed as

$$\begin{cases} \lambda_{\mathrm{PM},a} = \lambda_{\mathrm{PM},1}\cos(\theta) + \sum\limits_{v=2k+1} \lambda_{\mathrm{PM},v}\cos(v\theta - \theta_v) \\ \lambda_{\mathrm{PM},b} = \lambda_{\mathrm{PM},1}\cos\left(\theta - \dfrac{2\pi}{3}\right) + \sum\limits_{v=2k+1} \lambda_{\mathrm{PM},v}\cos\left(v\theta - \theta_v - 2v\dfrac{\pi}{3}\right) \\ \lambda_{\mathrm{PM},c} = \lambda_{\mathrm{PM},1}\cos\left(\theta + \dfrac{2\pi}{3}\right) + \sum\limits_{v=2k+1} \lambda_{\mathrm{PM},v}\cos\left(v\theta - \theta_v + 2v\dfrac{\pi}{3}\right) \end{cases} \quad (2)$$

where *k* is a positive integer, $\lambda_{\mathrm{PM},1}$ is the amplitude of the fundamental magnet flux, $\lambda_{\mathrm{PM},v}$ is the amplitude of the *v*th harmonic magnet flux, θ is the rotor electrical position, and θ_v is the angle between the *v*th harmonic magnet flux and the fundamental one.

III. Fault Diagnosis

It is known that the HRC may lead to the positive, negative and ZSVC and ZSCC in three stator windings. Therefore, the HRC can be detected by monitoring these components. In this paper, the HRC in the delta-connected PMSM is first detected by using the ZSCC. In addition, the previous literatures [11], [20]–[23] present the ZSCC method for the detection of the interturn and static eccentricity faults of the delta-connected machine. Hence, the combined use of the literatures [11], [20]–[23] and this paper for the HRC can separate these types of faults of the machine.

A. Approximate Expression of ZSCC

According to Kirchhoff's voltage law, the sum of three-phase voltages of a delta-connected PMSM is equal to zero, and expressed as

$$V_a + V_b + V_c = 0. \quad (3)$$

By substituting (1) into (3), it results in

$$R_s(i_a + i_b + i_c) + (L + 2M)\frac{d(i_a + i_b + i_c)}{dt} + R_{\mathrm{add\_}a} i_a + \frac{d}{dt}(\lambda_{\mathrm{PM},a} + \lambda_{\mathrm{PM},b} + \lambda_{\mathrm{PM},c}) = 0. \quad (4)$$

The ZSCC is defined as

$$i_{\mathrm{zsc}} = i_a + i_b + i_c. \quad (5)$$

By substituting (2) and (5) into (4), it yields

$$R_s i_{\mathrm{zsc}} + (L + 2M)\frac{di_{\mathrm{zsc}}}{dt} = -R_{\mathrm{add\_}a} i_a - \frac{d\lambda_{\mathrm{PM},0}}{dt} \quad (6)$$

where

$$\lambda_{\mathrm{PM},0} = \lambda_{\mathrm{PM},a} + \lambda_{\mathrm{PM},b} + \lambda_{\mathrm{PM},c} = 3\sum_{v=3n,n=1,3,5\cdots} \lambda_{\mathrm{PM},v}\cos(v\theta - \theta_v). \quad (7)$$

In a healthy PMSM, $R_{\mathrm{add\_}a}$ is equal to 0. Then, it can be seen from (6) that the i_{zsc} only depends on the time derivative of the $\lambda_{\mathrm{PM},0}$. Therefore, the i_{zsc} is only constituted by the $3n$ ($n = 1, 3, 5, \ldots$) order harmonic components. In the case of the HRC, i_{zsc} depends on the stator current i_a, besides the time derivative of the $\lambda_{\mathrm{PM},0}$. Here, the stator current i_a includes the fundamental component and other harmonic components. Hence, besides the $3n$ order harmonic components, the fundamental component and other harmonic components are present in the i_{zsc}. The amplitude of the fundamental component is the largest among those of the new added harmonic component. Consequently, the HRC may be detected by the fundamental component of the i_{zsc}.

Regardless of the high-order harmonic components in the stator currents, the stator current i_a is expressed as

$$i_a = I_a\sin(\theta + \theta_a) \quad (8)$$

where I_a and θ_a are the amplitude and initial phase angle of the stator current i_a, respectively.

Substituting (8) into (6) and neglecting the time derivative of the $\lambda_{\mathrm{PM},0}$ since only the fundamental component of the i_{zsc} is considered for fault diagnosis, it yields

$$R_s i_{\mathrm{zsc}} + (L + 2M)\frac{di_{\mathrm{zsc}}}{dt} = -R_{\mathrm{add\_}a} I_a\sin(\theta + \theta_a). \quad (9)$$

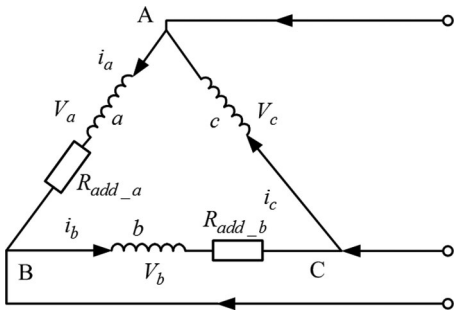

Fig. 2. Equivalent model of a delta-connected PMSM with HRC in the phases a and b.

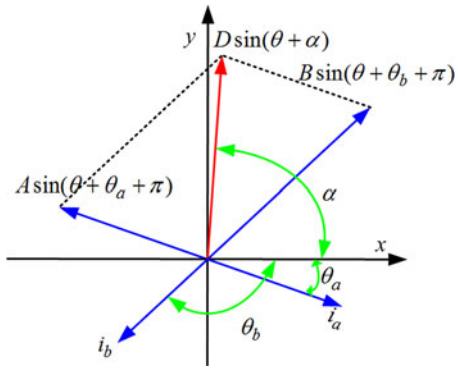

Fig. 3. Range of the angle α for the delta-connected PMSM with HRC in the phases a and b.

Then, (9) is changed into

$$R_s i_{\rm zsc} + \omega_s(L+2M)\frac{di_{\rm zsc}}{d\theta} = R_{\rm add\_a} I_a \sin(\theta+\theta_a+\pi) \tag{10}$$

where ω_s is the electrical angle speed of the PMSM.

In (10), if θ is regarded as an independent variable, and $i_{\rm zsc}$ is regarded as a dependent variable. Thus, (10) is a first order nonhomogeneous linear differential equation with constant coefficients. Hence, $i_{\rm zsc}$ can be calculated as

$$\begin{aligned} i_{\rm zsc} = & \frac{R_{\rm add\_a} I_a}{\sqrt{(\omega_s(L+2M))^2+R_s^2}}\sin(\theta+\theta_a+\pi+\gamma) \\ & + Ce^{\frac{-R_s}{\omega_s(L+2M)}\theta} \end{aligned} \tag{11}$$

where C is an arbitrary constant, and γ is a variable and expressed as

$$\gamma = \tan^{-1}(-\omega_s(L+2M)/R_s). \tag{12}$$

As θ tends to infinity, the second term at the right side of equal sign in (11) is close to 0. Hence, (11) is simplified as

$$\begin{aligned} i_{\rm zsc} &= \frac{R_{add\_a} I_a}{\sqrt{(\omega_s(L+2M))^2+R_s^2}}\sin(\theta+\theta_a+\pi+\gamma) \\ &= I_1\sin(\theta+\theta_1) \end{aligned} \tag{13}$$

where I_1 and θ_1 are defined as the amplitude and initial phase angle of the fundamental component in the $i_{\rm zsc}$, respectively, and they are expressed as

$$\begin{cases} I_1 = \dfrac{R_{add\_a} I_a}{\sqrt{(\omega_s(L+2M))^2+R_s^2}} \\ \theta_1 = \theta_a+\pi+\gamma. \end{cases} \tag{14}$$

As mentioned in [7], the most common HRC occurs in only one phase. Even so, the fault in two phases is considered to further verify the effectiveness of the method proposed in this paper. Fig. 2 shows that the fault occurs in the phases a and b simultaneously. In this case, the $i_{\rm zsc}$ can be still expressed in (13), but where I_1 and θ_1 are expressed as

$$\begin{cases} I_1 = \dfrac{D}{\sqrt{(\omega_s(L+2M))^2+R_s^2}} \\ \theta_1 = \alpha+\gamma \end{cases} \tag{15}$$

where

$$\begin{cases} A = R_{\rm add\_a} I_a \, B = R_{\rm add\_b} I_b \\ D = \sqrt{A^2+B^2+2AB\cos(\theta_a-\theta_b)} \\ \alpha = \arcsin\left(\dfrac{A\sin(\theta_a+\pi)+B\sin(\theta_b+\pi)}{D}\right) \end{cases} \tag{16}$$

where $R_{\rm add\_b}$ is the additional resistance in the phase b, and I_b and θ_b are the amplitude and initial phase angle of the fundamental component of the stator current i_b, respectively. Additionally, the range of the angle α in (15) and (16) for the HRC in the phases a and b is presented in Fig. 3, where the angle α is between $\theta_b+\pi$ and $\theta_a+\pi$. If the HRC only occurs in single phase, the angle α is $\theta_a+\pi$ and $\theta_b+\pi$ for fault phase a and fault phase b, respectively.

B. Fault Indicator and Angle Differences

Theoretically, I_1 may be used as a fault indicator. However, it is affected by the variation of the operating point of the PMSM, as seen from (15) and (16). Hence, a fault indicator without the influence of the operating point is greatly required. To overcome this problem, the Park's vector modulus is defined as

$$|\vec{i_s}| = \sqrt{i_d^2+i_q^2} \tag{17}$$

where i_d and i_q are the Park's vector components of the phase currents and expressed as

$$\begin{cases} i_d = \sqrt{\dfrac{2}{3}}i_a - \dfrac{1}{\sqrt{6}}i_b - \dfrac{1}{\sqrt{6}}i_c \\ i_q = \dfrac{1}{\sqrt{2}}i_b - \dfrac{1}{\sqrt{2}}i_c. \end{cases} \tag{18}$$

Regardless of the high-order harmonic components, the stator current i_a is expressed in (8), and the other two phase currents

of the three-phase PMSM are expressed as

$$\begin{cases} i_b = I_b \sin(\theta + \theta_b) \\ i_c = I_c \sin(\theta + \theta_c) \end{cases} \tag{19}$$

where I_c and θ_c are the amplitude and initial phase angle of the stator current i_c, respectively.

In a healthy PMSM, the following conditions are satisfied:

$$\begin{cases} I_a = I_b = I_c = I_m \\ \theta_b = \theta_a - 2\pi/3 \\ \theta_c = \theta_a + 2\pi/3 \end{cases} \tag{20}$$

where I_m is the amplitude of the stator currents. Hence, in the healthy PMSM, the Park's vector modulus is expressed as

$$|\overline{i_s}| = I_m \sqrt{\frac{3}{2}}. \tag{21}$$

The HRC in only one phase can be regarded as an especial case. Hence, the fault indicator of the HRC in two phases would be discussed. In the case of the HRC in two phases *a* and *b*, three-phase stator currents are mostly balanced as R_{add_a} and R_{add_b} are not very large. Here, I_a and I_b in (16) are both approximately equal to I_m, and the initial phase angle difference between i_a and i_b is approximately equal to $2\pi/3$, as shown in (20). Hence, the first row of (15) is transformed into

$$\begin{aligned} I_1 &= \frac{I_m \sqrt{R_{\mathrm{add}\_a}^2 + R_{\mathrm{add}\_b}^2 - R_{\mathrm{add}\_a} R_{\mathrm{add}\_b}}}{\sqrt{(\omega_s(L+2M))^2 + R_s^2}} \\ &= \frac{R_{\mathrm{add},e} I_m}{\sqrt{(\omega_s(L+2M))^2 + R_s^2}} \end{aligned} \tag{22}$$

where $R_{\mathrm{add},e}$ is the estimated resistance and expressed as

$$R_{\mathrm{add},e} = \sqrt{R_{\mathrm{add}\_a}^2 + R_{\mathrm{add}\_b}^2 - R_{\mathrm{add}\_a} R_{\mathrm{add}\_b}}. \tag{23}$$

The estimated resistance can be calculated by (22)

$$R_{\mathrm{add},e} = \frac{I_1 \cdot \sqrt{(\omega_s(L+2M))^2 + R_s^2}}{I_m}. \tag{24}$$

By combining (22) and (24), it can be seen that the estimated resistance $R_{\mathrm{add},e}$ is not affected by the operating point of the PMSM since the quantities I_m and ω_s are eliminated, neglecting the variations of the PMSM parameters (R_s, *L*, and *M*). To avoid calculating I_m in frequency domain, the relationship between I_m and Park's vector modulus is used. By substituting (21) into (24), it generates

$$R_{\mathrm{add},e} = \sqrt{\frac{3}{2}} \frac{I_1 \cdot \sqrt{(\omega_s(L+2M))^2 + R_s^2}}{|\overline{i_s}|}. \tag{25}$$

It is shown in (25) that the estimated resistance $R_{\mathrm{add},e}$ is independent on the faulty phases and operating point, which make $R_{\mathrm{add},e}$ as a reliable fault indicator. Hence, the fault can be detected by observing the variation of the fault indicator. To avoid the false detection, the fault indicator has to be compared to a preset threshold corresponding to its value for the healthy PMSM to remove the influence of the inherent asymmetry of the PMSM.

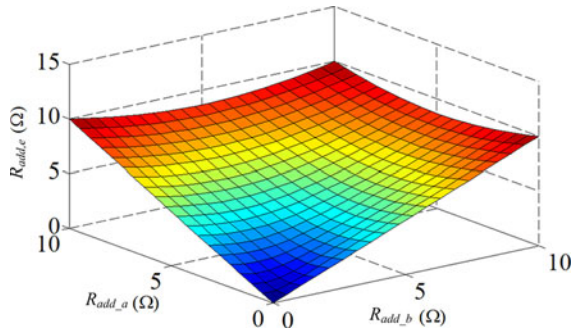

Fig. 4. Value of $R_{\mathrm{add},e}$ as a function of R_{add_a} and R_{add_b}.

Additionally, it can be noted that the value of $R_{\mathrm{add},e}$ is theoretically equal to the value of R_{add_a} according to (23) as the fault just occurs in the phase *a*. Then, the value of $R_{\mathrm{add},e}$ increases with the increase of the value of R_{add_a}. In the case of the fault in two phases *a* and *b*, the value of $R_{\mathrm{add},e}$ with the variation of R_{add_a} and R_{add_b} is presented in Fig. 4. It is shown that the value of R_{add_e} is not varied in the monotonic way.

In the case of the fault in two phases *a* and *b*, the initial phase angle difference of the fundamental components between the i_{zsc} and the phase current i_a is between $\pi/3+\gamma$ and $\pi+\gamma$ according to Fig. 3, (16) and (20). Furthermore, as the HRC only occurs in the phase *a*, the initial phase angle difference of the fundamental components between the i_{zsc} and the phase current i_a is equal to $\pi+\gamma$ theoretically. Similarly, the same results can be obtained as the fault occurs in other phases. Hence, angle difference d_j ($j = a, b, c$) is defined as

$$d_j = \begin{cases} |\theta_1 - \theta_j - \pi - \gamma| & |\theta_1 - \theta_j - \pi - \gamma| <= \pi \\ 2\pi - |\theta_1 - \theta_j - \pi - \gamma| & |\theta_1 - \theta_j - \pi - \gamma| > \pi. \end{cases} \tag{26}$$

According to (16), (20) and Fig. 3, the angle differences listed in Table I are theoretically satisfied under different fault conditions. Therefore, the faulty phases can be identified by observing the variations of the angle differences. In addition, R_{add_c} in Table I is the additional resistance in the phase *c*.

C. Frequency Tracking Algorithm

In order to achieve online diagnosis, the defined fault indicator and angle difference should be obtained in real time since one may do not know when the HRC would aggravate to the extent that the machine could not tolerate. As seen from (25) and (26), only the amplitude I_1 and initial phase angle θ_1 of the i_{zsc}, the initial phase angles of the fundamental components of the stator currents i_a, i_b, and i_c are required to be calculated in real time since R_s, *L*, and *M* are known constants, the variable ω_s already exists in the normal operation of the system, the Park's vector modulus and the angle γ can be directly calculated. In this study, an effective frequency tracking algorithm is applied to calculate the amplitude and initial phase angle of the fundamental component, where the calculation is not required in frequency domain.

TABLE I
ANGLE DIFFERENCES UNDER HRC CONDITION

	Fault in the phase *a*	
$d_a = 0$	$d_b = 2\pi/3$	$d_c = 2\pi/3$
	Fault in the phase *b*	
$d_a = 2\pi/3$	$d_b = 0$	$d_c = 2\pi/3$
	Fault in the phase *c*	
$d_a = 2\pi/3$	$d_b = 2\pi/3$	$d_c = 0$
	Fault in the phases *a* and *b*	
$R_{\mathrm{add}\_a} = R_{\mathrm{add}\_b}$	$R_{\mathrm{add}\_a} > R_{\mathrm{add}\_b}$	$R_{\mathrm{add}\_a} < R_{\mathrm{add}\_b}$
$d_a = \pi/3$	$0 < d_a < \pi/3$	$\pi/3 < d_a < 2\pi/3$
$d_b = \pi/3$	$\pi/3 < d_b < 2\pi/3$	$0 < d_b < \pi/3$
$d_c = \pi$	$2\pi/3 < d_c < \pi$	$2\pi/3 < d_c < \pi$
	Fault in the phases *b* and *c*	
$R_{\mathrm{add}\_b} = R_{\mathrm{add}\_c}$	$R_{\mathrm{add}\_b} > R_{\mathrm{add}\_c}$	$R_{\mathrm{add}\_b} < R_{\mathrm{add}\_c}$
$d_a = \pi$	$2\pi/3 < d_a < \pi$	$2\pi/3 < d_a < \pi$
$d_b = \pi/3$	$0 < d_b < \pi/3$	$\pi/3 < d_b < 2\pi/3$
$d_c = \pi/3$	$\pi/3 < d_c < 2\pi/3$	$0 < d_c < \pi/3$
	Fault in the phases *c* and *a*	
$R_{\mathrm{add}\_c} = R_{\mathrm{add}\_a}$	$R_{\mathrm{add}\_c} > R_{\mathrm{add}\_a}$	$R_{\mathrm{add}\_c} < R_{\mathrm{add}\_a}$
$d_a = \pi/3$	$\pi/3 < d_a < 2\pi/3$	$0 < d_a < \pi/3$
$d_b = \pi$	$2\pi/3 < d_b < \pi$	$2\pi/3 < d_b < \pi$
$d_c = \pi/3$	$0 < d_c < \pi/3$	$\pi/3 < d_c < 2\pi/3$

As expressed in (13), the i_{zsc} is constituted by the fundamental component. Transforming (13) into an orthogonal reference frame, the current components at *d*-axis and *q*-axis are defined as

$$\begin{cases} I_d = I_1 \sin(\theta + \theta_1)\cos(\theta) \\ I_q = I_1 \sin(\theta + \theta_1)\sin(\theta). \end{cases} \tag{27}$$

Using trigonometric identities and further calculation, then

$$\begin{cases} I_d = I_1[\sin(2\theta + \theta_1) + \sin(\theta_1)]/2 \\ I_q = -I_1[\cos(2\theta + \theta_1) - \cos(\theta_1)]/2. \end{cases} \tag{28}$$

Filtering the harmonic components of current signals from (28), it has

$$\begin{cases} I_{dl} = I_1 \sin(\theta_1)/2 \\ I_{ql} = I_1 \cos(\theta_1)/2 \end{cases} \tag{29}$$

where I_{dl} and I_{ql} are the dc components in I_d and I_q, respectively. The amplitude and initial phase angle are calculated as

$$\begin{cases} I_1 = 2\sqrt{I_{dl}^2 + I_{ql}^2} \\ \theta_1 = \tan^{-1}\left(\dfrac{I_{dl}}{I_{ql}}\right). \end{cases} \tag{30}$$

It can be seen from (30) that the amplitude and initial phase angle of the fundamental component in the i_{zsc} are calculated in real time, since the dc components I_{dl} and I_{ql} can be obtained in time domain.

D. Fault Diagnosis Steps

To further understand the proposed method, the online fault diagnosis steps are summarized as follows.

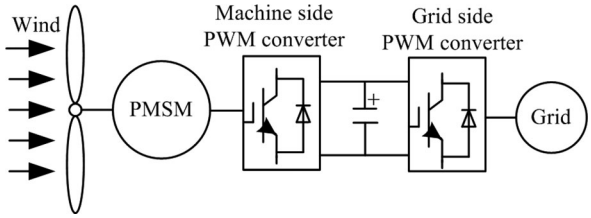

Fig. 5. Structure of the WECS.

Step 1: *Fault feature extraction*. The frequency tracking algorithm is adopted to calculate the amplitude I_1 and initial phase angle θ_1 of the fundamental component of the i_{zsc}, the initial phase angles θ_a, θ_b, and θ_c of the fundamental components of the phase currents i_a, i_b, and i_c. Then, the fault indicator and angle differences are calculated.
Step 2: *Fault detection*. If the fault indicator is larger than the preset threshold, the fault is detected. Then, the identification of the faulty phases is switched to *Step* 3. Otherwise, the process is switched to *Step* 1.
Step 3: *Fault location*. After the fault is detected, the faulty phases are identified based on the angle difference in (26).

IV. SIMULATION

In this paper, the application of PMSM to the WECS as an example is used to validate the proposed method. In industrial applications, a WECS with wind turbine (WT) and PMSM is shown in Fig. 5, where the WT is connected to the PMSM directly. The electrical power generated by the PMSM is transmitted to a power grid through a full size back to back PWM converter, consisting of a machine-side converter (MSC) and a grid-side converter (GSC) [24]. Additionally, the control of the PWM converter is simple as the MSC may be operated in separated with the GSC. Hence, only the MSC is considered in this paper.

As a real WECS is one high-power system, it is difficult to verify the proposed method in a real WECS directly. To keep the consistency of the simulation and experimental conditions, the proposed method is verified in a reduced-scale simulation and experiment platforms. The simulation model of WT as well as the implementation of the proposed method is carried out based on MATLAB/Simulink, as shown in Fig. 6, which mainly includes WT and generator.

The imitation of WT is indispensable in the simulation and experiment for the WECS. The PMSM-1 with wye-connected windings in Fig. 6 is applied to imitate WT with the rated power 180 W based on the imitation principle of WT. In this case, $i_d = 0$ control strategy employing current hysteresis controller is used to control the PMSM-1, as shown in Fig. 6. The PMSM-2 with the delta-connected windings in Fig. 6, operating at generator mode, is directly driven by the PMSM-1. The control method of the PMSM-2 consists of two control loops, namely inner loop and outer loop. The inner loop current controller regulates the stator currents of the PMSM-2. The outer loop speed PI controller tracks the optimal shaft speed reference expressed in (31) to generate the maximum power point tracking from WT

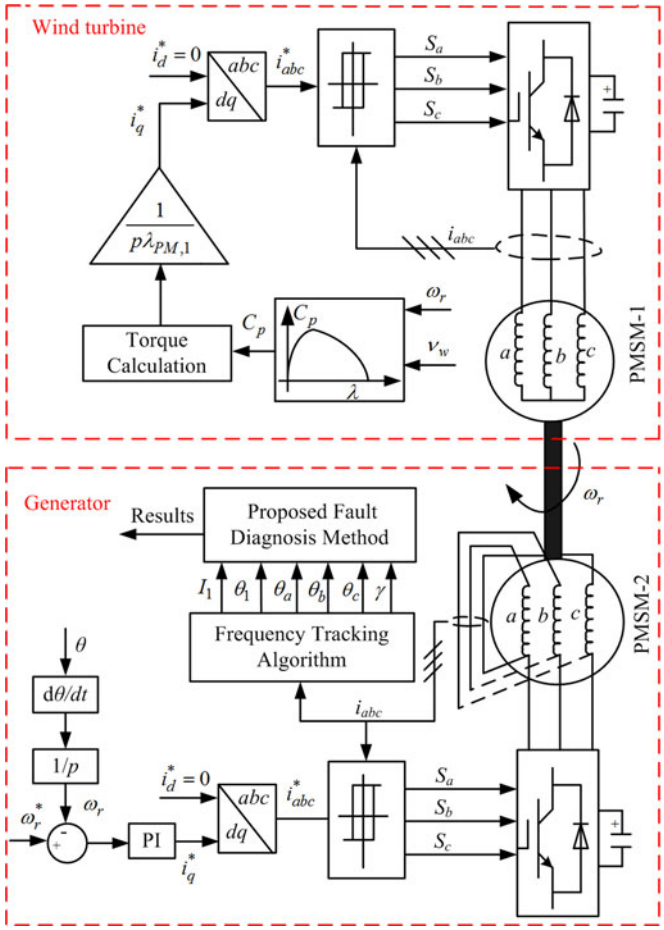

Fig. 6. Simulation model of the WT with the proposed fault diagnosis method.

TABLE II
SPECIFIC PARAMETERS OF WT AND PMSM

WT	Value	PMSM	Value
Rated Wind Speed (m/s)	6	Number of pole pairs	2
Blade Radius (m)	0.94	Stator Resistance (Ω)	10.5
Optimal Tip Speed Ratio	8.1	Self-inductance (H)	0.13
Air Density (k/m^3)	1.225	Mutual-inductance (H)	−0.03
Optimal Power Coefficient	0.48	Permanent Magnet Flux Linkage (Wb)	0.636

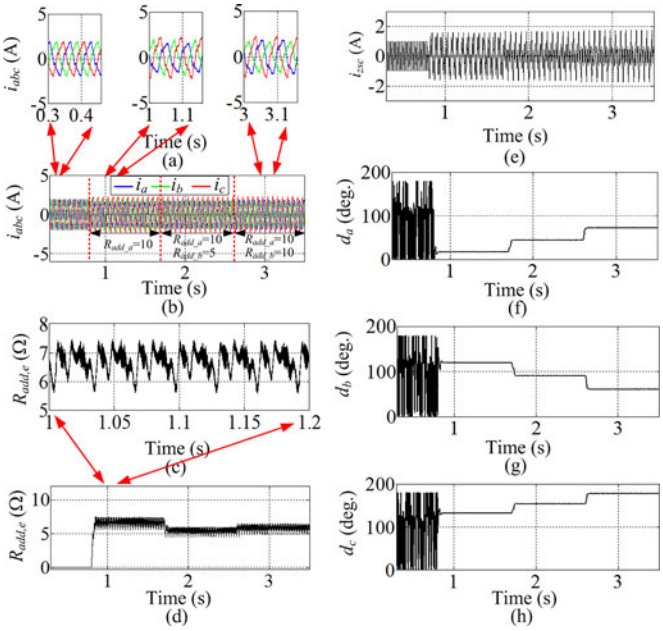

Fig. 7. Simulation results for the HRC in phases a and b. (a) i_{abc}. (b) i_{abc}. (c) $R_{\mathrm{add},e}$. (d) $R_{\mathrm{add},e}$. (e) i_{zsc}. (f) d_a. (g) d_b. (h) d_c.

[24]:

$$\omega_r^* = \frac{\lambda_{\mathrm{opt}} v_w}{R} \tag{31}$$

where λ_{opt} is the optimal tip speed ratio, v_w is the wind speed, and R is the blade radius of WT. $i_d = 0$ control strategy employing current hysteresis controller is adopted to control the PMSM-2 due to the simplicity and effectiveness [25].

In the simulation, the PMSM model is established based on the voltage equations in *abc* reference frame, as introduced in Section II, which can allow one to modify all the parameters of the machine to simulate any fault conditions. The HRC is simulated by means of the additional resistances connected in series with stator phase windings. The parameters of WT and PMSMs are listed in Table II, and the parameters of the PMSM-1 and PMSM-2 are the same. In the simulation, the wind speed is 5.83 m/s.

Fig. 7 shows the simulation results for the HRC in the phases a and b. At $t = 0.8$ s, an additional resistance $R_{\mathrm{add}\_a} = 10\Omega$ is connected in the phase a, and other phases keep healthy. As a result, the fault indicator converges into a value near 6.6 Ω with period oscillation, and d_a, d_b, and d_c are approximately equal to $\pi/10$, $2\pi/3$, and $3\pi/4$, respectively. Another fault in the phase b ($R_{\mathrm{add}\_b} = 5\Omega$) is introduced at $t = 1.7$ s, besides R_{add_a} is equal to 10 Ω. As a consequence, the estimated resistance converges to a value near to 5.4, and d_a, d_b, and d_c are changed into $\pi/4$, $\pi/2$, and $6\pi/7$, respectively. At $t = 2.6$ s, R_{add_b} increases to 10 Ω and R_{add_a} keeps unvaried. In consequence, the estimated resistance increases to a value near to 5.8, and d_a, d_b, and d_c are close to $2\pi/5$, $\pi/3$, and π, respectively. It can be seen that the fault indicator and angle differences have certain differences from the theoretical values under fault conditions. The reason may be that the three-phase currents are not balanced as the HRC occurs, as shown in Fig. 7(a). On the other hand, the harmonic components are not considered during the theoretical analysis. However, this will not make it difficult to detect the fault and identify the faulty phases since the fault indicator is obviously larger than the threshold, and angle differences are close to the theoretical values under different fault conditions.

As mentioned in Section III-B, the fault can be detected independently of the phases in which the fault occurs by the proposed method. The other two simulations are performed with the identical faults in the phases b and c, c and a, and the similar results are shown in Figs. 8 and 9. As seen from Figs. 7–9, the fault can be properly detected in the three cases, being independent on the faulty phases. Additionally, the faulty phases can be identified by using the angle differences.

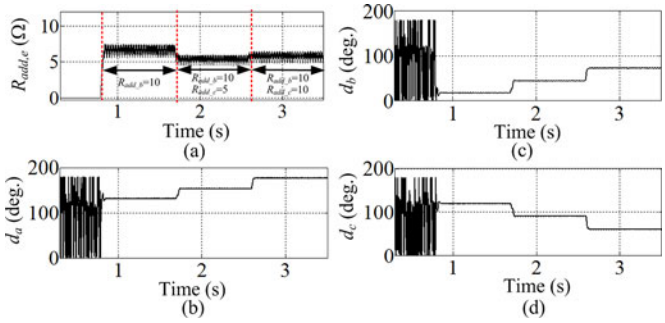

Fig. 8. Simulation results for the HRC in phases b and c. (a) $R_{\mathrm{add},e}$. (b) d_a. (c) d_b. (d) d_c.

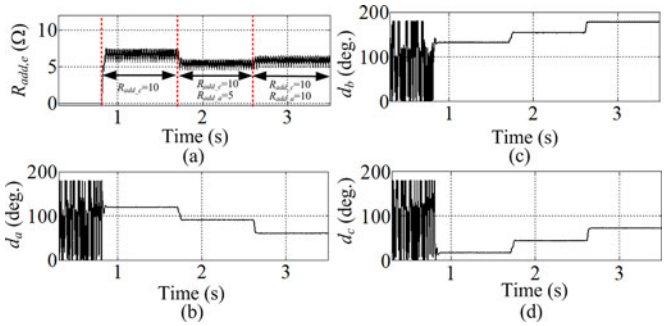

Fig. 9. Simulation results for the HRC in phases c and a. (a) $R_{\mathrm{add},e}$. (b) d_a. (c) d_b. (d) d_c.

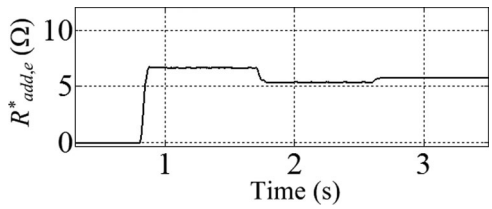

Fig. 10. Mean of the sliding window for the HRC in the phases a and b.

Moreover, it can be noticed from Figs. 7–9 that the period oscillations are present in the estimated resistance as the fault occurs, which may affect the fault diagnosis performance. To deal with this issue, the mean of the sliding window defined in [26] is expressed in (32), and used as a new fault indicator to take benefits of its filtering characteristic, reducing the oscillations

$$R^{*}_{\mathrm{add},e}(m\cdot T)=\frac{1}{N}\sum_{i=m-N+1}^{m}R_{\mathrm{add},e}(i\cdot T)N=\frac{T_e}{2T} \quad (32)$$

where T is sampling period, T_e is the electrical period of the stator current, and k is an integer number.

Fig. 10 shows the mean of sliding window for the fault presented in Fig. 7. It is shown that the oscillation of the estimated resistance is obviously decreased comparing with the result in Fig. 7(d).

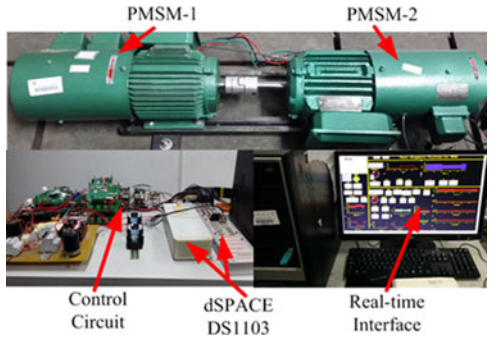

Fig. 11. Experimental platform.

V. Experimental Validation

A. Experimental Platform

To further validate the proposed method, the experimental platform is setup, as shown in Fig. 11, which mainly includes two PMSMs with the same parameters, a three-phase diode bridge rectifier, two three-phase voltage source inverters, a dSPACE DS1103, a controlled resistance, voltage sensors, current sensors, and an incremental encoder with 1024 pulses per revolution. The PMSM-1 is used for the imitation of WT, directly driving the PMSM-2 with the delta-connected windings. The measured voltages, currents, and the signal of the encoder are fed into the dSPACE DS1103. The controlled resistance is used to keep relatively constant dc voltage in the generator side. The control methods used for the PMSM-1 and PMSM-2 are the same as those in the simulation. All the switching commands are generated by the dSPACE DS1103. The parameters of the PMSMs are listed in Table II.

In this experiment, the HRC is emulated with the resistance boxes connected in series with the stator phase windings. In the previous literatures [7], the additional resistance is equal to the value of the rated phase resistance. In this paper, in order to validate the sensitivity of the proposed method, the additional resistance is set in seven different values during the experiments, namely 15.2% (1.6 Ω), 22.8% (2.4 Ω), 30.5% (3.2 Ω), 38% (4 Ω), 47.6% (5 Ω), 66.6% (7 Ω), 95.2% (10 Ω) of the rated phase resistance value.

B. Steady-State Condition

In order to perform a better comparison, the same faults in the simulation are modeled in this section. Fig. 12 shows the experimental results for the HRC in the phases a and b, where the wind speed is 5.83 m/s.

At $t = 6.4$ s, the first fault is generated, where an additional resistance $R_{\mathrm{add\_}a} = 10\ \Omega$ is connected in the phase a, and other phases keep healthy. A simultaneous fault ($R_{\mathrm{add\_}a} = 10\ \Omega$ and $R_{\mathrm{add\_}b} = 5\ \Omega$) is introduced at $t = 15.4$ s. At $t = 25.2$ s, $R_{\mathrm{add\_}b}$ increases to 10 Ω, and $R_{\mathrm{add\_}a}$ is still equal to 10 Ω. It can be seen from Fig. 12 that all the variables show the similar behavior with the simulation ones in Figs. 7 and 10.

It may be seen that there is a little difference between experimental results and simulation ones. First, it can be seen that the

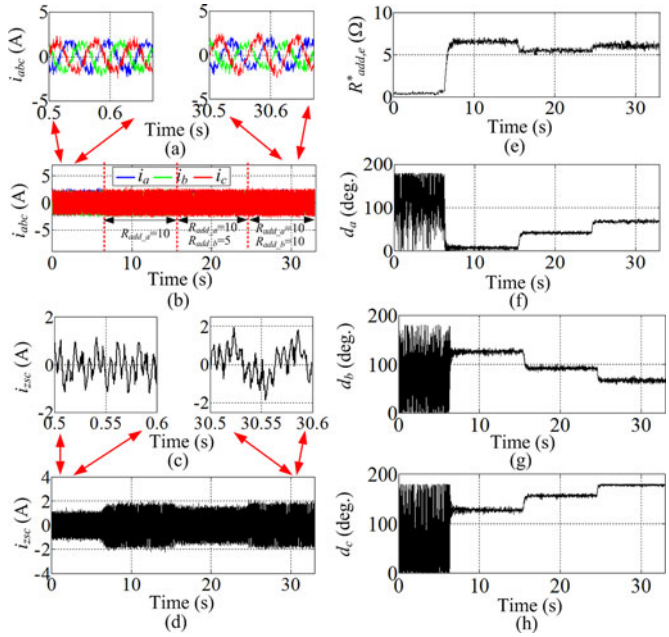

Fig. 12. Experimental results for the HRC in the phases a and b. (a) i_{abc}. (b) i_{abc}. (c) i_{zsc}. (d) i_{zsc}. (e) $R^*_{\mathrm{add},e}$. (f) d_a. (g) d_b. (h) d_c.

fault indicator is larger than 0 under normal condition and the fault indicator is not the same as the one in the simulation under fault condition. The differences between experiment results and simulation ones may generate from the inherent asymmetry of the machine. Second, as the fault occurs, the angle differences seem noisier than those in the simulation and are a little different from those in the simulation, where the reason may be that the measurement interferences of the current sensors and the saturation of the machine are not considered in the simulation.

The experimental results in Fig. 12 show that the proposed method can diagnose the fault and identify the faulty phases even if the experimental results are a little different from the simulation ones and theoretical analysis.

C. Dynamic Condition

To validate the performance of the proposed method, the experiments are carried out with stochastic wind model, where the mean wind speed is 6 m/s. Fig. 13 shows the experimental waveforms of the wind speed and stator currents together with the fault indicator and angle differences, where the additional resistance $R_{\mathrm{add\_}a} = 10\ \Omega$ is connected in the phase a of the PMSM-2. It is shown that the amplitudes of the stator currents change with the fluctuation of wind speed. The mean of sliding window and angle differences are not significantly affected by the fluctuation of wind speed, which is in agreement with the theoretical analysis. Hence, the experimental results indicate that the HRC can be still detected and identified under the condition of the stochastic wind.

D. Performance Evaluation of the Fault Diagnosis Method

Fig. 14 shows the fault indicator and angle differences versus additional resistance ($R_{\mathrm{add\_}a}$), where the additional resistance

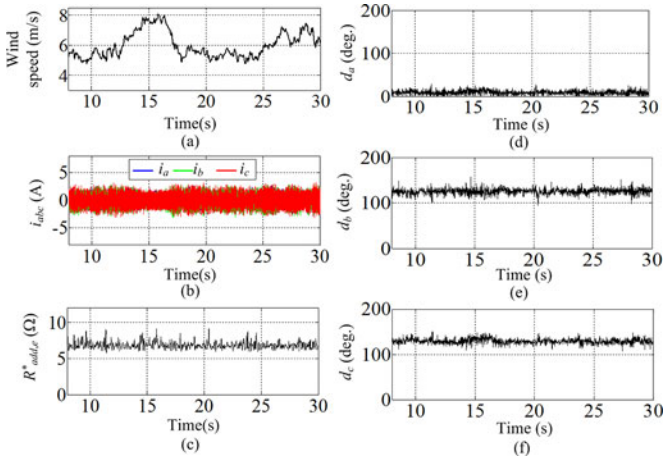

Fig. 13. Experimental results for the HRC in phase a. (a) Wind speed. (b) i_{abc}. (c) $R^*_{\mathrm{add},e}$. (d) d_a. (e) d_b. (f) d_c.

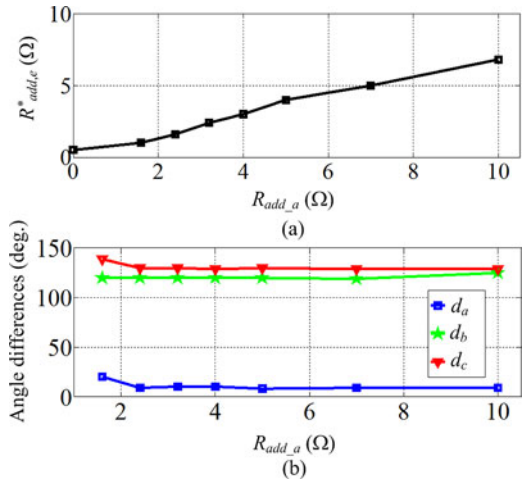

Fig. 14. Fault indicator ($R^*_{\mathrm{add},e}$) and angle differences versus additional resistance ($R_{\mathrm{add\_}a}$). (a) $R^*_{\mathrm{add},e}$. (b) Angle differences.

is connected in the phase a of the PMSM-2 and wind speed is 5.83 m/s. As seen from Fig. 14(a), the increase of the additional resistance produces an increase in the value of the fault indicator. Hence, the fault severity may be assessed from the value of the fault indicator. Moreover, it is important to note that as the additional resistance ($R_{\mathrm{add\_}a} = 1.6\ \Omega$) is very small, the fault indicator (equal to 1) is still larger than the threshold (equal to 0.5), as shown in Fig. 14(a). This indicates that the fault can be still detected and show the sensitivity of the proposed method to the variation of the additional resistance even for its smaller value. On the other hand, it can be seen from Fig. 14(b) that the angle differences are almost unaffected with the increase in the value of the additional resistance, indicating that the faulty phases may be effectively identified.

VI. Conclusion

This paper first proposes an online method for diagnosing the HRC in the delta-connected PMSM using the ZSCC. The

theoretical analysis is presented, and the fault indicator and angle differences are defined. An effective frequency tracking algorithm is applied to calculate the amplitude and initial phase angle of the fundamental component, and, then, the fault indicator and angle differences are obtained. Finally, the fault is diagnosed by combination of the fault indicator and angle differences. To validate the proposed method, the simulation and experiment have been carried out. From the theoretical analysis, simulation, and experimental results, the following conclusions can be drawn:

1) the fault detection and fault severity estimation can be implemented by observing the variation of the fault indicator (mean of sliding window);
2) the faulty phases can be identified according to the angle differences of the fundamental components between the ZSCC and the stator currents;
3) the fault indicator and angle differences are not significantly affected by the variation of the operating point of the PMSM.

REFERENCES

[1] M. Cheng and Y. Zhu, "The state of the art of wind energy conversion systems and technologies: A review," *Energy Convers. Manage.*, vol. 88, pp. 332–347, Dec. 2014.

[2] W. Wang, M. Cheng, B. Zhang, Y. Zhu, and S. Ding, "A fault-tolerant permanent magnet traction module for subway application," *IEEE Trans. Power Electron.*, vol. 29, no. 4, pp. 1646–1658, Apr. 2014.

[3] Z. Hameed, Y. S. Hong, Y. M. Cho, S. H. Ahn, and C. K. Song, "Condition monitoring and fault detection of wind turbines and related algorithms: A review," *Renew. Sustainable Energy Rev.*, vol. 13, no. 1, pp. 1–39, Jan. 2009.

[4] J. Hang, J. Zhang, M. Cheng, and Z. Wang, "Fault diagnosis of mechanical unbalance for permanent magnet synchronous motor drive system under nonstationary condition," in *Proc. IEEE Energy Convers. Congr. Expo.*, Denver, CO, USA, Sep. 15–19, 2013, pp. 3556–3562.

[5] P. M. De La Barrera, G. R. Bossio, and J. A. Solsona, "High-resistance connection detection in induction motor drives using signal injection," *IEEE Trans. Ind. Electron.*, vol. 61, no. 7, pp. 3563–3573, Jul. 2014.

[6] L. M. Popa, B. B. Jensen, F. Ritche, and I. Boldea, "Condition monitoring of wind generators," in *Proc. IEEE Conf. Rec. Annu. Meet. Ind. Appl.*, Oct. 12–16, 2003, pp. 1839–1846.

[7] Y. Gritli, L. Zarri, C. Rossi, and F. Filippetti, "Advanced diagnosis of electrical faults in wound-rotor induction machines," *IEEE Trans. Ind. Electron.*, vol. 60, no. 9, pp. 4012–4024, Sep. 2013.

[8] W. Yang, P. J. Tavner, C. J. Crabtree, and M. Wilkinson, "Cost-effective condition monitoring for wind turbines," *IEEE Trans. Ind. Electron.*, vol. 57, no. 1, pp. 263–271, Jan. 2010.

[9] F. V. Santos, M. G. Riera, H. Henao, and M. S. Pineda, "Diagnosis of rotor and stator asymmetries in wound rotor induction machines under nonstationary operation through the instantaneous frequency," *IEEE Trans. Ind. Electron.*, vol. 6, no. 9, pp. 4947–4959, Sep. 2014.

[10] S. Nandi, H. A. Toliyat, and X. D. Li, "Condition monitoring and fault diagnosis of electrical motors—A review," *IEEE Trans. Energy Convers.*, vol. 20, no. 4, pp. 719–729, Dec. 2005.

[11] J. Hang, J. Zhang, M. Cheng, and J. Huang, "Online interturn fault diagnosis of permanent magnet synchronous machine using zero-sequence components," *IEEE Trans. Power Electron.*, vol. 30, no. 12, pp. 6731–6741, Dec. 2015.

[12] D. Yao, X. Shi, and M. Krishnamurthy, "A new approach to fault diagnostics for permanent magnet synchronous machines using electromagnetic signature analysis," *IEEE Trans. Power Electron.*, vol. 28, no. 8, pp. 4104–4112, Aug. 2013.

[13] J. B. He, C. Somogyi, A. Strandt, and N. A. O. Demerdash, "Diagnosis of stator winding short-circuit faults in interior permanent magnet synchronous machine," in *Proc. IEEE Energy Convers. Congr. Expo.*, Sep. 14–18, 2014, pp. 3125–3130.

[14] W. Le Roux, R. G. Harley, and T. G. Habetler, "Detecting rotor faults in low power permanent magnet synchronous machines," *IEEE Trans. Power Electron.*, vol. 22, no. 1, pp. 322–328, Jan. 2007.

[15] B. M. Ebrahimi, M. Javan Roshtkhari, J. Faiz, and S. V. Khatami, "Advanced eccentricity fault recognition in permanent magnet synchronous motors using stator current signature analysis," *IEEE Trans. Ind. Electron.*, vol. 61, no. 4, pp. 2041–2052, Apr. 2014.

[16] J. C. Urresty, J. R. Riba, and L. Romeral, "Influence of the stator windings configuration in the currents and zero-sequence voltage harmonics in permanent magnet synchronous motors with demagnetization faults," *IEEE Trans. Magn.*, vol. 49, no. 8, pp. 4885–4893, Aug. 2013.

[17] X. Xiao, C. M. Chen, and M. Zhang, "Dynamic permanent magnet flux estimation of permanent magnet synchronous machines," *IEEE Trans. Appl. Supercond.*, vol. 20, no. 3, pp. 1085–1088, Jun. 2010.

[18] J. C. Urresty, "Electrical and magnetic faults diagnosis in permanent magnet synchronous motors," Ph.D. dissertation, Dept. Electr. Eng., Polytechnic Univ. Catalonia, Barcelona, Spain, Jun. 2012.

[19] E. Schmidt, M. Susic, and A. Eilenberger, "Design studies on a permanent magnet synchronous machine with Y- and Δ-connected stator winding," *IEEE Trans. Mag.*, vol. 47, no. 5, pp. 1042–1045, May 2011.

[20] A. Sayed-Ahmed and N. A. O. Demerdash, "Fault-tolerant operation of delta-connected scalar- and vector-controlled ac motor drives," *IEEE Trans. Power Electron.*, vol. 27, no. 6, pp. 3041–3049, Jun. 2012.

[21] F. Briz, M. W. Degner, P. Garcia, and A. B. Diez, "Induction machine diagnostics using zero sequence components," in *Proc. 14th Annu. Meet. Conf. Rec. Ind. Appl.*, Oct. 2–6, 2005, pp. 34–41.

[22] K. N. Gyftakis and J. C. Kappatou, "The zero-sequence current as a generalized diagnostic mean in Δ-connected three-phase induction motors," *IEEE Trans. Energy Convers.*, vol. 29, no. 1, pp. 1–11, Mar. 2014.

[23] K. N. Gyftakis and J. C. Kappatou, "A novel and effective method of static eccentricity diagnosis in three-phase PSH induction motors," *IEEE Trans. Energy Convers.*, vol. 28, no. 2, pp. 405–412, Jun. 2013.

[24] Q. Wei, X. Yang, and X. Gong, "Wind speed and rotor position sensorless control for direct-drive PMG wind turbines," *IEEE Trans. Ind. Appl.*, vol. 48, no. 1, pp. 3–11, Jan./Feb. 2012.

[25] N. M. A. Freire, J. O. Estima, and A. J. M. Cardoso, "Open-circuit fault diagnosis in PMSG drives for wind turbine application," *IEEE Trans. Ind. Electron.*, vol. 60, no. 9, pp. 3957–3967, Sep. 2013.

[26] B. Aubert, J. Regnier, S. Caux, and D. Alejo, "Stator inter-turn short-circuit detection in permanent magnet synchronous generators using extended Kalman filtering," in *Proc. IEEE Electron., Control, Meas., Signals Appl. Mechatron. Conf.*, Toulouse, France, Jun. 24–26, 2013, pp. 1–6.

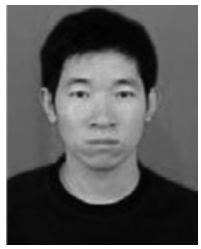

Jun Hang (S'12) received the B.Sc. and M.Sc. degrees in electrical engineering from the Anhui University of Science and Technology, Huainan, China, in 2008 and 2011, respectively. He is currently working toward the Ph. D degree in electrical engineering at Southeast University, Nanjing, China.

His current research interests include condition monitoring, fault diagnosis, and wind power generation.

Jianzhong Zhang (M'08) received the M.Sc. and Ph.D. degrees in electrical engineering from the Department of Electrical Engineering, Southeast University, Nanjing, China, in 2005 and 2008, respectively.

Since 2008, he has been with Southeast University, where he is currently a Research Professor at the School of Electrical Engineering. In recent years, he has authored and coauthored more than 80 technical papers and 25 Chinese patents. His research interests include electric machines, power electronics, and wind power generation.

Ming Cheng (M'01–SM'02–F'15) received the B.Sc. and M.Sc. degrees from the Department of Electrical Engineering, Southeast University, Nanjing, China, in 1982 and 1987, respectively, and the Ph.D. degree from the Department of Electrical and Electronic Engineering, The University of Hong Kong, Hong Kong, in 2001.

Since 1987, he has been with Southeast University, where he is currently a Professor at the School of Electrical Engineering and the Director at the Research Center for Wind Power Generation. His teaching and research interests include electrical machines, motor drives for electric vehicles, and renewable energy generation. He has authored or coauthored more than 300 technical papers and four books and is the holder of 60 patents in these areas.

Prof. Cheng is a Fellow of the Institution of Engineering and Technology. He has served as the Chair and Organizing Committee Member for many international conferences. He is a Distinguished Lecturer of the IEEE Industry Applications Society in 2015/2016.

Bangfu Zhang (S'13) received the B.S. degree in electrical engineering from Huaqiao University, Xiamen, China, in 2010. He has been working toward the Ph.D. degree in electrical engineering at Southeast University, Nanjing, China, since 2011.

In 2014, he was a joint Ph.D. Student founded by the China Scholarship Council with the Department of Electronic and Electrical Engineering, University of Sheffield, Sheffield, U.K., where he worked on linear permanent-magnet motors design for vertical transportation application. His research interests include design, analysis, and control of linear permanent magnet machines.

Shichuan Ding (S'08–S'12) received the B.Sc. degree in electrical engineering from Anhui University, Hefei, China, in 2001, and the M.Sc. degree from USTC, Hefei, China, in 2006. He is currently working toward the Ph.D. degree in electrical engineering at Southeast University, Nanjing, China.

His research interests include electrical machine drive, power electronics applications, and energy management in EVs.